

# Online Reliable Anomaly Detection via Neuromorphic Sensing and Communications

Junya Shiraishi, *Member, IEEE*, Jiechen Chen, *Member, IEEE*, Osvaldo Simeone, *Fellow, IEEE*, and Petar Popovski, *Fellow, IEEE*

**Abstract**—This paper proposes a low-power online anomaly detection framework based on neuromorphic wireless sensor networks, encompassing possible use cases such as brain–machine interfaces and remote environmental monitoring. In the considered system, a central reader node actively queries a subset of neuromorphic sensor nodes (neuro-SNs) at each time frame. The neuromorphic sensors are event-driven, producing spikes in correspondence to relevant changes in the monitored system. The queried neuro-SNs respond to the reader with impulse radio (IR) transmissions that directly encode the sensed local events. The reader processes these event-driven signals to determine whether the monitored environment is in a normal or anomalous state, while rigorously controlling the false discovery rate (FDR) of detections below a predefined threshold. The proposed approach employs an online hypothesis testing method with  $\epsilon$ -values to maintain FDR control without requiring knowledge of the anomaly rate, and it dynamically optimizes the sensor querying strategy by casting it as a best-arm identification problem in a multi-armed bandit framework. Extensive performance evaluation demonstrates that the proposed method can reliably detect anomalies under stringent FDR requirements, while efficiently scheduling sensor communications and achieving low detection latency.

**Index Terms**—anomaly detection, false discovery rate control, hypothesis test, multi-armed bandit, neuromorphic sensing and communication.

## I. INTRODUCTION

Neuromorphic technologies – encompassing sensing [1], [2], computing [3], [4], and communication [5], [6], [7], [8], [9], [10] – are emerging as a promising paradigm for ultra-low-power, low-latency sensor networks. Inspired by the brain’s event-driven information processing, a neuromorphic sensor records information by producing spikes at times marking significant changes in the monitored environment [11]. Thanks to the inherent capacity of neuromorphic sensors to respond only to relevant events, incorporating neuromorphic sensors in a remote monitoring system can drastically reduce

J. Shiraishi and J. Chen contributed equally to this work. The work of J. Shiraishi was supported by European Union’s Horizon Europe research and innovation funding programme under Marie Skłodowska-Curie Action (MSCA) Postdoctoral Fellowship, “NEUTRINAL” with grant agreement No. 101151067. The work of J. Chen and O. Simeone was supported by the EPSRC project EP/X011852/1, and O. Simeone was also supported by an Open Fellowships of the EPSRC (EP/PW024101/1). The work of P. Popovski was supported by the Velux Foundation, Denmark, through the Villum Investigator Grant WATER, nr. 37793. (*Corresponding author: Jiechen Chen*)

J. Shiraishi and P. Popovski are with the Department of Electronic Systems, Aalborg University, 9220 Aalborg, Denmark (e-mail: {jush, petarp}@es.aau.dk). J. Chen and O. Simeone are with the King’s Communications, Learning and Information Processing Laboratory, King’s College London, WC2R 2LS London, U.K. (e-mail: {jiechen.chen, osvaldo.simeone}@kcl.ac.uk)

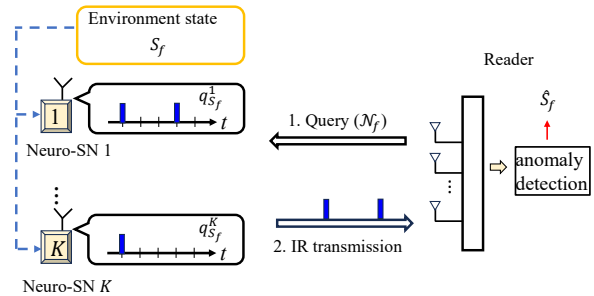


Fig. 1: In the setup under study, a reader interrogates a subset  $\mathcal{N}_f$  of the  $K$  neuromorphic sensor nodes (neuro-SN) at each frame  $f$  in order to determine whether the behavior of the monitored system is normal or anomalous. The binary variable  $S_f$  indicates the presence or absence of an anomaly at frame  $f$ , while  $\hat{S}_f$  represents the corresponding estimate of the reader.

redundant transmissions, leading to substantial energy and bandwidth savings and supporting the deployment of large populations of wireless sensors [5], [10].

For example, reference [10] demonstrated an asynchronous wireless network of salt-grain-sized sensors that mimic neural spikes, showing that hundreds of microscale nodes can communicate sporadic bursts of data to a central receiver using backscattering. Such neuromorphic networks have been highlighted for their potential in brain–machine interfaces, where implantable sensors would relay neural spikes in real time, as well as in other domains like wearable devices and environmental sensing [12].

In applications such as remote surveillance and autonomous systems, timely detection of abnormal events is critical. Notably, neuromorphic vision sensors can detect sudden motion or the appearance of an intruder – e.g., an unauthorized drone – by producing rapid spikes, while remaining largely inactive under normal conditions [1]. In environmental monitoring, distributed sensors might pick up abrupt changes in temperature or smoke indicative of a forest fire [13]. In these scenarios, the system must provide reliable anomaly detection despite limited energy supply and communication bandwidth.

To this end, the detection algorithm needs to be statistically robust, minimizing false alarms to avoid wasting attention and energy on benign events. Furthermore, the network must intelligently decide which sensors to query and when, so as to maximize the chance of detecting an anomaly while conserving resources. In this regard, a common reliability criterion is maintaining the *false discovery rate (FDR)* below

a target level, ensuring that only a small fraction of reported anomalies are false positives [14], [15], [16]. Achieving a low FDR is especially important in safety-critical applications, like health monitoring or security, to maintain trust in the system’s alarms.

This paper addresses these challenges by proposing a novel solution that integrates tools from statistical FDR control [17] and adaptive learning [18] into a neuromorphic wireless sensing framework.

### A. Related Work

*Neuromorphic sensing:* Neuromorphic sensing aims to emulate biological sensory systems by encoding information through sparse, event-driven signals rather than continuous streams. A prominent category is vision sensing, where dynamic vision sensors (DVSs) detect asynchronous changes in brightness at each pixel, achieving low latency and high energy efficiency. Prophesee and IniVation are among the leading companies in this area, offering state-of-the-art event-based cameras for machine vision and robotic applications [19], [20]. Beyond vision, companies like SynSense are developing ultra-low-power neuromorphic processors such as Speck, which enable local event-driven processing for embedded intelligence [21].

*Neuromorphic communication:* Recent work [6] has introduced end-to-end neuromorphic communication systems that replaces conventional sensing and frame-based radio with a fully spike-driven pipeline. In it, neuromorphic sensors produce asynchronous event spikes which are encoded by a spiking neural network (SNN) and transmitted as impulse radio (IR) pulses, then decoded by another SNN at the receiver. This all-spike design was shown to significantly lower latency and improve efficiency compared to conventional synchronous digital communication.

Building on this, reference [5] extended the approach to a multi-user, fading-channel scenario. In it, each internet of things (IoT) device uses a neuromorphic event sensor, on-device SNN, and IR transmitter, communicating over a shared wireless channel to a receiver that also employs an SNN. A key principle in these systems is event-driven data acquisition, which allows the wireless network to inherently focus on the “semantics” of the data – i.e. changes that carry new information – rather than sending redundant raw readings.

Further energy savings can be obtained by combining IR-based communication with wake-up radio triggers [7], adopting different design criteria [22], and leveraging multi-level spikes [9]. In particular, reference [9] shows that associating each spike with a small payload can improve inference accuracy without increasing spike count. This study also includes an experimental evaluation using software-defined radios.

*Online anomaly detection:* Online anomaly detection focuses on identifying abnormal patterns in streaming data in real time, without requiring access to the entire dataset beforehand. For example, reference [14] proposed online false discovery rate control methods for anomaly detection in time

series to address the challenges of rare anomalies and temporal dependencies. Reference [15] proposed an unsupervised real-time anomaly detection algorithm for streaming data, which is capable of continuous learning and early detection of both spatial and temporal anomalies without requiring labeled data or batch processing.

*Multi-armed bandit optimization:* Multi-armed bandit (MAB) optimization has been extensively studied in previous works. For example, reference [18] proposed the track-and-stop strategy for best-arm identification under fixed-confidence settings. Reference [23] studied the complexity of best-arm identification in stochastic MAB under both fixed-budget and fixed-confidence settings. To speed up the convergence of MAB in unseen tasks, [24] proposed for the first time the use of contextual meta-learning that incorporates auxiliary optimization tasks knowledge.

### B. Main Contributions

Building on the above context and prior art, this paper develops a protocol for online anomaly detection via neuromorphic sensor networks. The main contributions are summarized as follows:

- *Online anomaly detection framework based on neuromorphic sensors:* We introduce a novel online anomaly detection system based on neuromorphic sensor networks. As shown in Fig. 1, this model implements a pull-based communication strategy, where a central reader intermittently queries neuromorphic sensor nodes and receives event-driven IR spike signals. The model explicitly incorporates the sparse, asynchronous nature of neuromorphic data and the requirement to control the false discovery rate in detection decisions.
- *Adaptive FDR control with e-values:* We design an adaptive statistical testing framework that guarantees FDR control at any desired level in an online setting. In contrast to traditional methods that rely on fixed p-value thresholds, our framework utilizes e-values [25] to accumulate evidence over each frame. This allows the detector to flexibly adjust its confidence as new spike data arrive, ensuring that the expected proportion of false alarms remains below the target level even when the anomaly occurrence rate is unknown and nonstationary.
- *Best-arm identification for sensor scheduling:* We introduce a sensor scheduling policy based on best-arm identification principles from multi-armed bandit theory [18]. At each time frame, the reader must decide which sensors to query next. Our policy dynamically learns the sensors that are most likely to yield an anomaly indication by treating each sensor as an ‘arm’ with an unknown reward. By continuously updating estimates and concentrating queries on the most promising sensor, the policy achieves efficient allocation of limited query opportunities, accelerating the detection of anomalies under uncertainty.
- *Extensive performance evaluation:* We provide a thorough performance evaluation of the proposed system

through analysis and simulations. The results demonstrate that our approach can detect anomalies quickly and reliably under a variety of conditions. In particular, we show that the FDR is maintained below the target level in all tested scenarios, validating the effectiveness of the  $\epsilon$ -value based control. Moreover, the adaptive scheduling policy is shown to significantly reduce detection delay and resource usage compared to non-adaptive or random scheduling baselines.

The rest of the paper is organized as follows. Section II describes the pull-based neuromorphic wireless communications system, while the online anomaly detection based on hypothesis test framework is described in Section III. Section IV explains the scheduling policy optimization based on best-arm identification. Experimental setting and results are described in Section V. Finally, Section VI concludes the paper.

## II. SYSTEM MODEL

### A. Setting

Fig. 1 shows the basic setup considered in this paper. We consider a pull-based neuromorphic wireless communications scenario where the reader conducts a continuous online anomaly detection at each time frame based on the deployment of neuromorphic sensor nodes (neuro-SN) [10].

The  $K$  neuro-SNs observe a common environment via local neuromorphic sensors [5], and communicate with the reader via IR. We define the set of node indices by  $\mathcal{K} = \{1, 2, \dots, K\}$ . Through communication with the neuro-SNs, the reader continuously monitors the environment to detect anomalies, while ensuring that the FDR is maintained below a pre-determined level, denoted as  $\alpha$ . The FDR measures the fraction of detected anomalies that do not correspond to actual anomalies. Specific applications include real-time forest fire detection [13] or drone activity monitoring [5] based on wireless sensor networks.

As in [14], anomalies are defined as rare events that significantly deviate from expected patterns. In our setting, an anomaly causes neuromorphic sensors to produce spikes, also known as events, at a significantly higher rate than under normal conditions. For example, neuromorphic cameras produce spikes at times in which activity is recorded in the monitored scene [5]. Thus, in the presence of significant activity, e.g., from unauthorized drones, the spike rate is increased.

As illustrated in Fig. 2, we adopt a discrete time model, in which time is divided into frames indexed by  $f = 1, 2, \dots, F$ . Each frame consists of three phases:

- 1) *Downlink query signal transmission*: At the beginning of each frame, the reader first sends a query signal to a selected subset of devices.
- 2) *Sensing and uplink IR transmission*: Upon detecting the query signal, e.g., via a wake-up radio [7], [26], a neuro-SN activates its neuromorphic sensor and its IR transmitter. The IR transmission phase is divided into

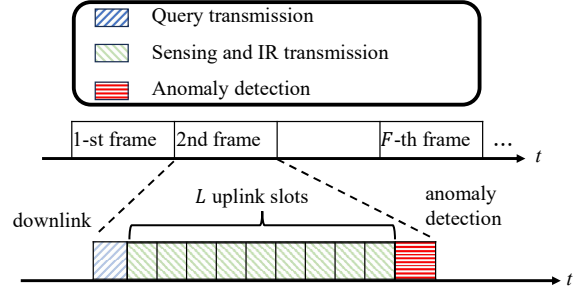


Fig. 2: Frame structure illustrating the query transmission from the reader (downlink), sensing and impulse radio (IR) transmission by the selected neuro-SN during  $L$  uplink slots, and anomaly detection at the reader.

$L$  time slots, during which the neuro-SNs sense and transmit in an online and event-driven manner.

- 3) *Anomaly detection at the reader*: Finally, the reader determines whether the environment is in an anomalous state based on the received signals.

### B. Observation Models

Following [14], we model the presence or absence of an anomaly in a frame indexed by  $f$  as an arbitrary, unknown sequence of binary state  $S_f$ , which are defined as

$$S_f = \begin{cases} 0, & \text{no anomaly,} \\ 1, & \text{anomaly.} \end{cases} \quad (1)$$

We model the observations of each neuromorphic sensor  $k$  at the  $f$ -th frame via a Bernoulli process with spiking rate determined by the current state  $S_f$ . Accordingly, for each sensor  $k$ , we set two spiking rates corresponding to the absence or presence of an anomaly, namely,  $q_0^k$  and  $q_1^k$ . As illustrated in Fig. 3, we assume the inequality  $q_0^k \leq q_1^k$  for all  $k \in \{1, 2, \dots, K\}$ . This indicates that anomalies are characterized by larger spiking rates.

Accordingly, each node  $k$  obtains a spike sequence  $s_f^k = [s_{f,1}^k, \dots, s_{f,L}^k] \in \{0, 1\}^L$ , where  $s_{f,l}^k = 1$  indicates that node  $k$  records a spike at time instant  $l$  of the  $f$ -th frame, and  $s_{f,l}^k = 0$  indicates that no spike was recorded. This means that we have

$$s_{f,l}^k \underset{\text{i.i.d.}}{\sim} \text{Bern}(q_f^k) \text{ with } q_f^k = \begin{cases} q_0^k & \text{if } S_f = 0 \\ q_1^k & \text{if } S_f = 1. \end{cases} \quad (2)$$

Through an initial calibration phase, the reader can obtain the statistics on the spike rates in normal conditions. Therefore, the reader is assumed to know the value of the probability  $q_0^k$  for all  $k \in \{1, 2, \dots, K\}$ . In contrast, we assume the reader does not know the spiking probability  $q_1^k$  in the presence of anomalies.

### C. Scheduling and Impulse Radio Transmission

In this work, we assume time division multiple access (TDMA)-based communication between the reader and neuro-SNs, which consists of downlink phase and uplink phases.

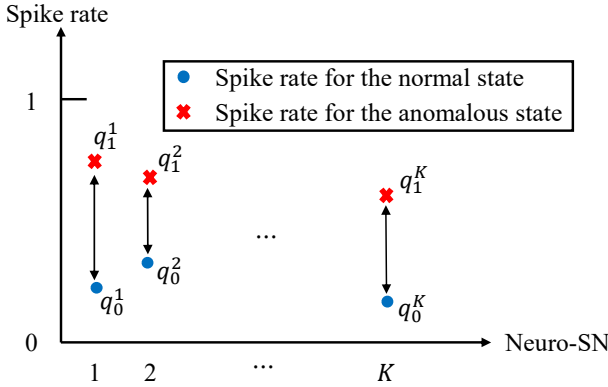


Fig. 3: Each  $k$ -th sensor is characterized by a known spiking probability  $q_0^k$  in normal conditions, and a higher, unknown spiking probability  $q_1^k \geq q_0^k$  in the presence of an anomaly.

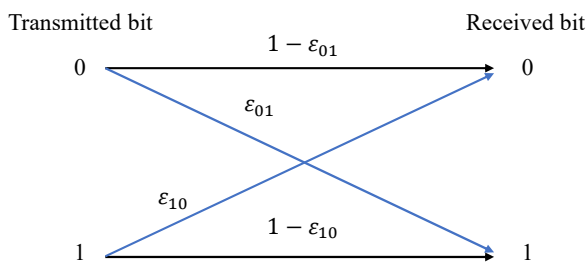


Fig. 4: Illustration of a binary asymmetric channel.

At each time frame  $f$ , the reader requests data from a subset  $\mathcal{N}_f \subseteq \{1, \dots, K\}$  of neuro-SN by multicasting a query signal that encodes the target node IDs and its schedule information. The reader schedules  $|\mathcal{N}_f| = C_{\max}$  nodes, and transmits this control information during the downlink phase. In practice, the cardinality  $C_{\max}$  of the scheduled set depends on the available uplink capacity.

The nodes that receive the query signal begin sensing over the  $L$  time instants within the frame. The spike sequence  $s_f^k$  is transmitted by all scheduled sensors in  $\mathcal{N}_f$  in an online and event-driven manner using IR by directly mapping a spike from the sensor to an electromagnetic pulse [5].

As illustrated in Fig. 4, we model the channel as a binary asymmetric channel, where transmitted bits may be flipped at the receiver, with bit 0 flipping to 1 with probability  $\epsilon_{01}$ , and bit 1 flipping to 0 with probability  $\epsilon_{10}$ . The IR receiver at the reader estimates the spike sequence transmitted by each neuro-SN. After receiving the estimated spike sequence  $\hat{s}_f^k = [\hat{s}_{f,1}^k, \dots, \hat{s}_{f,L}^k] \in \{0, 1\}^L$  for each node  $k \in \mathcal{N}_f$  at time frame  $f$ , the reader uses this information to determine whether the current state  $S_f$  is normal or anomalous, as described in the next section.

### III. ONLINE ANOMALY DETECTION

In this section, we first present the hypothesis test framework, assuming that the reader has collected data from the subset of nodes  $\mathcal{N}_f$  at the  $f$ -th frame. Then, we describe the

proposed anomaly detection mechanism for online anomaly detection. The problem of optimizing node scheduling will be addressed in the next section.

#### A. Hypothesis Testing Framework

At the end of each frame  $f$ , the reader tests whether the current system state is normal or anomalous. Specifically, it considers the following hypothesis

$$\mathcal{H}_f : S_f = 0 \text{ (normal state)} \quad (3)$$

against the alternative hypothesis that there is an anomaly, i.e.,  $S_f = 1$ . Equivalently, the reader evaluates the null hypothesis for the requested sensors in  $\mathcal{N}_f$  as follows

$$\mathcal{H}_f : s_f^k \stackrel{\text{i.i.d.}}{\sim} \text{Bern}(q_0^k), \forall k \in \mathcal{N}_f \quad (4)$$

against the composite alternative hypothesis

$$\bar{\mathcal{H}}_f : s_f^k \stackrel{\text{i.i.d.}}{\sim} \text{Bern}(q_1^k), \text{ for some } q_1^k > q_0^k, \forall k \in \mathcal{N}_f. \quad (5)$$

In order to conduct a hypothesis test during the  $f$ -th frame, the reader uses the spike sequences  $\hat{s}_f = \{\hat{s}_f^k\}_{k \in \mathcal{N}_f}$  observed during this frame and creates the test statistics  $X_f$ . In addition, the reader selects the rejection threshold  $\alpha_f$  by considering the target metrics, such as FDR. The null hypothesis  $\mathcal{H}_f$  is that there is no anomaly, such that if this hypothesis is rejected, the reader declares an anomalous state. The decision at frame  $f$  is denoted as  $\hat{S}_f \in \{0, 1\}$ , which can be described as  $\hat{S}_f = h(X_f, \alpha_f)$ . Here,  $h(X_f, \alpha_f)$  is an indicator function representing the rejection decision based on  $X_f$  and  $\alpha_f$ . In the following subsection, we first describe our target metrics and use test statistics based on e-values. Finally, we describe how to select the rejection thresholds  $\alpha_f$  considering the target metrics.

#### B. Decaying Memory Time-Averaged False Discovery Rate

Let  $\mathcal{F}_{f|0}$  represent the subset of the frame indices  $\{1, 2, \dots, f\}$  for which the environment is in a normal state, i.e.,  $\mathcal{F}_{f|0} = \{f' \in \{1, 2, \dots, f\} : S_{f'} = 0\}$ . At frame  $f$ , the cumulative number of anomalies declared by the reader, averaged with a forgetting factor  $0 < \delta < 1$  over the past frames, is

$$\hat{A}_f = \sum_{f'=1}^f \delta^{f-f'} \mathbb{1}(\hat{S}_{f'} = 1), \quad (6)$$

where  $\mathbb{1}(\cdot)$  is the indicator function, which equals to 1 if the argument is true, and equals to 0 otherwise. In a similar way, the weighted time-average of incorrectly detected anomalies is

$$F_f = \sum_{f'=1}^f \delta^{f-f'} \mathbb{1}(\hat{S}_{f'} = 1) \mathbb{1}(S_{f'} = 0). \quad (7)$$

We are interested in controlling the decaying-memory time-averaged FDR, which is defined as the ratio [14]

$$\text{FDR}_f = \mathbb{E} \left[ \frac{F_f}{\max(\hat{A}_f, 1)} \right], \quad (8)$$

This quantity measures the fraction of estimated anomalies that were actually normal states. Thus, controlling the FDR in (8) ensures that the system does not cause an excessive fraction of false alarms. Accordingly, the design target is to determine a sequence of rejection thresholds  $\{\alpha_f\}_{f=1}^{\infty}$  ensuring that the metric  $\text{FDR}_f$  is controlled below a pre-determined level  $\alpha$ , as

$$\text{FDR}_f \leq \alpha, \text{ for all frames } f = 1, \dots, F. \quad (9)$$

### C. Decaying Memory Time-Averaged True Discovery Rate

The bound in (9) can be trivially guaranteed by setting  $\alpha_f = 0$  for all frames  $f$ . In this case, no anomalies are detected, and thus there is no false detection of anomalies. However, this approach clearly fails to detect any potential anomalies. Therefore, a testing strategy must be also evaluated in terms of its ability to detect true anomalies. To account for this, we consider the true discovery rate (TDR) as the average fraction of truly anomalous states that are correctly detected.

In a similar way to the decaying-memory time-averaged FDR, let  $A_f$  denote the cumulative number of anomalies that occur in the environment at frame  $f$ , averaged with a forgetting factor  $0 < \delta < 1$ , which is defined as

$$A_f = \sum_{f'=1}^f \delta^{f-f'} \mathbb{1}(S_{f'} = 1). \quad (10)$$

Similarly, the weighted time-averaged of correctly detected anomaly, denoted as  $T_f$  can be expressed as

$$T_f = \sum_{f'=1}^f \delta^{f-f'} \mathbb{1}(\hat{S}_{f'} = 1) \mathbb{1}(S_{f'} = 1). \quad (11)$$

Finally, we define decayed-memory time-averaged TDR, which is defined as the ratio, as described below:

$$\text{TDR}_f = \mathbb{E} \left[ \frac{T_f}{\max(A_f, 1)} \right]. \quad (12)$$

This quantity measures how many actual anomaly events the reader successfully detects. This depends on the scheduling policy, which will be described in Sec. IV.

The metrics FDR in (8) and TDR in (12) will be used as a basis for designing rejection threshold  $\alpha_f$ . Specifically, in each frame, the reader sets a rejection threshold  $\alpha_f$  based on the past rejection history so that FDR condition in (9) is always guaranteed while providing high TDR. Specific algorithms should be designed by taking into account the well-known piggybacking and  $\alpha$  death problem [14], whose details are specified in Sec. III-E.

### D. Construction of E-Values

An e-value  $e_f \in [0, \infty]$  is a function of the current observations  $S_f$  that satisfies the inequality  $\mathbb{E}[e_f] \leq 1$  when the null hypothesis  $\mathcal{H}_f$  is true, i.e., when the state is normal ( $S_f = 0$ ) [25]. To construct an e-value  $e_f$  for each time frame

$f$ , the reader estimates the spike rate from node  $k$  at the  $f$ -th frame as

$$\hat{q}_f^k = \frac{1}{L} \sum_{l=1}^L \hat{s}_{f,l}^k. \quad (13)$$

Intuitively, a larger estimated rate  $\hat{q}_f^k$  suggests a higher likelihood that the environment is experiencing an anomaly.

Since the anomalous spike rates are unknown to the reader, an e-value can be constructed by relying on the plug-in method [25] along with the merging of e-values for the scheduled sensors  $k \in \mathcal{N}_f$ . Specifically, for each sensor  $k \in \mathcal{N}_f$ , an e-value is obtained via the likelihood ratio

$$e_f^k = \left( \frac{\hat{\psi}_{f|1}^k}{\hat{\psi}_{f|0}^k} \right)^{L \hat{q}_f^k} \left( \frac{1 - \hat{\psi}_{f|1}^k}{1 - \hat{\psi}_{f|0}^k} \right)^{L(1 - \hat{q}_f^k)}, \quad (14)$$

where

$$\psi_{f|0}^k = q_0^k (1 - \epsilon_{10}) + (1 - q_0^k) \epsilon_{01} \quad (15)$$

is the spiking probability that the reader receives from the neuro-SN  $k$  at the  $f$ -th frame when the environment is normal state and  $\hat{\psi}_{f|1}^k$  is the maximum likelihood of received spike rate at the reader from neuro-SN  $k$  at the  $f$ -th frame when the environment is anomalous state. This is obtained as

$$\hat{\psi}_{f|1}^k = \hat{q}_1^k (1 - \epsilon_{10}) + (1 - \hat{q}_1^k) \epsilon_{01}, \quad (16)$$

where  $\hat{q}_1^k$  is the maximum likelihood estimate of the spike rate  $q_1^k$ , which is given by

$$\hat{q}_1^k = \max(q_0^k, \hat{q}_f^k). \quad (17)$$

Finally, the reader merges the e-values  $\{e_f^k\}_{k \in \mathcal{N}_f}$  to obtain a single e-value via the arithmetic mean [25]

$$\bar{e}_f(\mathcal{N}_f) = \frac{1}{|\mathcal{N}_f|} \sum_{k \in \mathcal{N}_f} e_f^k. \quad (18)$$

### E. Design of the Rejection Thresholds

In order to ensure FDR condition (9), we adopt the algorithm detailed in [14]. Accordingly, at the end of each time frame  $f$ , the reader dynamically controls the decision threshold  $\alpha_f$  based on the past rejection history. An anomaly is declared if the statistic  $e_f$  is larger than a threshold  $1/\alpha_f$ , i.e.,

$$\hat{S}_f = \mathbb{1} \left( e_f > \frac{1}{\alpha_f} \right). \quad (19)$$

To describe the update of the threshold  $\alpha_f$ , let  $\rho_j$  denote the time of  $j$ -th detected anomaly, i.e.,

$$\rho_j = \min \left\{ f \geq 0 \mid \sum_{f'=1}^f \mathbb{1} \left( e_{f'} > \frac{1}{\alpha_{f'}} \right) \geq j \right\}, \quad (20)$$

and let  $\{\gamma_f\}_{f=1}^{\infty}$  denote a non-increasing sequence summing to 1, where  $\gamma_f = 0$  for all  $f \leq 0$ . We specifically use the default sequence [14]

$$\gamma_f \propto \frac{\log(\max(f, 2))}{f \exp(\sqrt{\log(f)})}. \quad (21)$$

Finally, let  $\tilde{\gamma}_f = \max(\gamma_f, 1 - \delta)$  as in [14]. Then, the rejection threshold  $\alpha_f$  is updated as

$$\alpha_f = \alpha \eta \tilde{\gamma}_f + \alpha \sum_{j \geq 1} \delta^{f - \rho_j} \gamma_{f - \rho_j}, \quad (22)$$

where  $\eta$  is smoothing parameter  $\eta > 0$ .

**Proposition 1** [14]. *When the decision threshold  $\alpha_f$  is updated according to (22) at each frame  $f$ , the anomaly detection rule in (19) ensures that the decaying-memory time-averaged FDR defined in (8) is controlled at level  $\alpha$  for all frames  $f$ , thus satisfying condition (9).*

#### IV. SCHEDULING POLICY OPTIMIZATION

In order to increase the TDR while maintaining FDR control as in (9), an ideal scheduling policy would select at each frame  $f$  the subset  $\mathcal{N}_f$  of sensors  $k$  with the highest spiking rates  $q_1^k$  under an anomalous state. In fact, this would maximize the chance of correctly detecting an anomaly via the test (19). However, the true spiking rates  $q_1^k$ , for  $k \in \mathcal{K}$ , are not known by the reader. Furthermore, anomalies occur arbitrarily and unpredictably, making it challenging to estimate the probabilities  $q_1^k$ .

In this section, we address the problem of optimizing the set  $\mathcal{N}_f$  by tackling these challenges. To start, we study the problem of identifying the best sensor

$$k^* = \arg \max_{k \in \mathcal{K}} q_1^k, \quad (23)$$

thus concentrating on the case  $C_{\max} = |\mathcal{N}_f| = 1$ , in which the uplink channel supports the transmission of a single neuro-SN. In this context, formally, the goal in this section is to minimize the number of frames used to identify the best neuro-SN  $k^*$  with a probability of error not exceeding a threshold  $\delta_s \in (0, 1)$ . An extension to any uplink capacity  $C_{\max} \geq 1$  will be also provided at the end of this section.

##### A. Multi-Armed Bandit Formulation

To facilitate the design of a scheduling policy, we make the working assumption that the anomaly process is i.i.d. across the frame index  $f$ , with an unknown anomalous probability  $\pi_1$ , i.e.,  $S_f \sim \text{Bern}(\pi_1)$ . Furthermore, we also assume that the normal spiking probabilities of all neuro-SNs are equal, i.e.,

$$q_0^k = q_0, \quad (24)$$

for all  $k = 1, \dots, K$ . Under these simplified assumptions, the spike rates  $\frac{1}{L} \sum_{l=1}^L s_{f,l}^k$  of each neuro-SN  $k$  is i.i.d. across frames  $f$ , with an average

$$\mu^k = (1 - \pi_1)q_0 + \pi_1 q_1^k. \quad (25)$$

This implies that the problem (23) of identifying the best sensor becomes equivalent to the problem of finding a node whose average spike rate  $\mu^k$  is the highest. i.e.,

$$k^* = \arg \max_{k \in \mathcal{K}} \mu^k. \quad (26)$$

This optimization can be formulated as the fastest best arm identification problem, studied in [18]. As demonstrated therein, a strategy known as track-and-stop reviewed next, is optimal.

##### B. Track-and-Stop Strategy

At each  $f$ -th frame, the reader estimates the spike rate  $\mu^k$  of neuro-SN  $k$  as

$$\hat{\mu}_f^k = \frac{1}{N_f^k} \sum_{f'=1}^f \hat{q}_{f'}^k \mathbb{1}(k \in \mathcal{N}_{f'}), \quad (27)$$

with

$$N_f^k = \sum_{f'=1}^f \mathbb{1}(k \in \mathcal{N}_{f'}) \quad (28)$$

being the number of frames in which neuro-SN  $k$  was scheduled and with  $\hat{q}_{f'}^k$  defined in (13).

Define as  $\mathbf{U}_f = \{k : N_f^k < \sqrt{f} - \frac{K}{2}\}$  the subset of nodes that have been scheduled fewer than  $\sqrt{f} - \frac{K}{2}$  times up to frame  $f$ . If this set is not empty, the track-and-stop strategy selects one of the neuro-SNs that was scheduled least frequently, i.e., in the smallest number of frames, emphasizing exploration [18]. Otherwise, the scheduling selection accounts also for the current spiking rate estimates  $\hat{\mu}_f = \{\hat{\mu}_f^1, \hat{\mu}_f^2, \dots, \hat{\mu}_f^K\}$ , considering both exploitation and exploration. Overall, the scheduling decision is

$$n_f = \begin{cases} \arg \min_{k \in \mathcal{K}} N_f^k, & \text{if } |\mathbf{U}_f| > 0, \\ \arg \min_{k \in \mathcal{K}} \{N_f^k - f \cdot w_{\sigma(k)}(\hat{\mu}_f)\}, & \text{otherwise,} \end{cases} \quad (29)$$

where  $\sigma : \{1, 2, \dots, K\} \rightarrow \{1, 2, \dots, K\}$  is a function that returns the rank of each node  $k$  in terms of the estimated spike rate  $\hat{\mu}^k$  in descending order, satisfying the inequalities  $\hat{\mu}_f^{\sigma(1)} \geq \hat{\mu}_f^{\sigma(2)} \dots \geq \hat{\mu}_f^{\sigma(K)}$ . The function  $w_{\sigma(k)}(\hat{\mu}_f)$ , which returns positive value, is detailed in [18] and satisfies the following property is true:  $w_1(\mu) \geq \dots \geq w_K(\mu)$ . This way, neuro-SNs with a larger estimated spiking rate are prioritized by the selection rule (29).

##### C. Extension of the Scheduling for Any Scheduling Capacity

In this subsection, we extend the track-and-stop strategy to the case where it is possible to schedule  $C_{\max} = |\mathcal{N}_f| \geq 1$  neuro-SNs. To this end, we propose that, at the beginning of each frame, the reader selects  $C_{\max} = |\mathcal{N}_f|$  nodes for scheduling by recursively applying the track-and-stop method in (29). Specifically, the reader selects the scheduled nodes one-by-one, obtaining the set  $\mathcal{N}_f = \{n_f^i\}_{i=1}^{C_{\max}}$ . In more detail, define  $\mathbf{U}_f^i = \{k \in \mathcal{K} \setminus \{n_f^j\}_{j=1}^{i-1} : N_f^k < \sqrt{f} - \frac{K}{2}\}$  as the set of neuro-SNs not yet included in the set  $\mathcal{N}_f$  that have been scheduled in the past frames fewer than  $\sqrt{f} - \frac{K}{2}$  times.

Then, the  $i$ -th scheduling node at the  $f$ -th frame is selected by applying the rule (29) as

$$n_f^i = \begin{cases} \arg \min_{k \in \mathcal{K} \setminus \{n_f^j\}_{j=1}^{j=i-1}} N_f^k, & \text{if } |\mathcal{U}_f^i| > 0, \\ \arg \min_{k \in \mathcal{K} \setminus \{n_f^j\}_{j=1}^{j=i-1}} N_f^k - fw_{\sigma(k)}(\hat{\mu}_f), & \text{otherwise,} \end{cases} \quad (30)$$

where function  $w_{\sigma(k)}(\cdot)$  is as defined in (29).

## V. NUMERICAL RESULTS

In this section, we present numerical results to validate the performance of the proposed online anomaly detection system.

### A. Simulation Setting

In our experiments, the anomaly process  $S_f$  is i.i.d. across all frames  $f$ , so that at each frame  $f$  the environment is in the anomalous state with probability  $\pi_1$  and in the normal state with probability  $1 - \pi_1$ , independently from frame to frame. We simulate a setting in which, as in (24), the spike rate  $q_0^k$  of a normal state is the same across all nodes, i.e.,  $q_0^k = q_0$  for all  $k \in \mathcal{K}$ . In contrast, the spiking rate  $q_1^k$  under the anomalous state is uniformly generated within the interval  $[q_0, q_0 + \Delta_{\max}]$  for each neuro-SN  $k$ . Table I shows our default parameters setting, which are used throughout the experiments unless stated otherwise.

TABLE I: Default parameter setting.

Parameters	Values
Number of neuro-SN $K$	5
Forgetting factor $\delta$	0.99 [14]
$\eta$	0.99
Number of uplink slots $L$	50
Target FDR $\alpha$	0.1 [14]
Simulation runs	$10^3$
Spiking rate under the normal state $q_0$	0.10
Anomaly ratio $\pi_1$	0.05
Error rates $(\epsilon_{01}, \epsilon_{10})$	$(0, 0)$
Upper bound on the spiking probability $\Delta_{\max}$	0.5
Channel capacity $C_{\max}$	1

### B. On the Validity of Online Anomaly Detection

We first investigate the validity of the online anomaly detection algorithm introduced in Sec. III. To this end, we compare the performance of the proposed scheme with adaptive threshold  $\alpha_f$  described in (22) with a more conventional fixed-threshold strategy, in which we apply the threshold  $\alpha_f = \alpha$  for all  $f \in [1, F]$ . Note that this combined approach does not satisfy the theoretical statistical guarantee in (9), and its performance can only be evaluated via numerical results.

Fig. 5 shows FDR and TDR versus the time frame  $f$  for fixed anomaly threshold method and for the proposed dynamic anomaly detection method in (22), where we set the number of neuro-SN  $K = 1$ . As anticipated, the fixed-threshold is not able to always satisfies the FDR constraint in (9). This is because this approach does not take into account the past rejection history for the current anomaly decision tasks. A fixed threshold can achieve a higher TDR than the

proposed method, but only by violating the FDR constraint in (9). In contrast, the introduced methodology, dynamic threshold always satisfies the FDR constraint  $\alpha$ , validating Proposition 1.

Fig. 6 shows the FDR and TDR as a function of the anomaly probability  $\pi_1$ , where we set  $K = 1$  and  $F = 1000$ . We observe that the fixed-threshold approach suffers from the higher FDR when the anomaly probability  $\pi_1$  is small, while the proposed dynamic anomaly detection threshold method can always satisfy the FDR constraint. When the anomaly probability  $\pi_1$  is small, with a dynamic threshold, the reader takes a conservative decision by setting a relatively smaller threshold  $\alpha_f$ , will a fixed-threshold method cannot adjust to the anomaly probability.

### C. Random v.s. Track-and-Stop Scheduling

We now study the impact of the scheduling strategy. To this end, Fig. 7 shows the FDR and the TDR versus the time frame  $f$  for the proposed anomaly detection scheme under a random scheduling strategy that selects  $C_{\max}$  neuro-SNs uniformly at random at every frame and for the track-and-stop method presented in Sec. IV. We set the parameters described in Table I with the uplink channel capacity  $C_{\max} = \{1, 2\}$  and anomaly probability  $\pi_1 = 0.1$ .

All schedulers, when coupled with the proposed anomaly detection, are seen to satisfy the FDR requirements, confirming the theoretical results in Proposition 1. Moreover, the figure highlights the benefits of track-and-stop, increasing the TDR for both uplink capacities  $C_{\max} = 1$  and  $C_{\max} = 2$ . This advantage stems from the capacity of track-and-stop to select the neuro-SNs that are most likely to contribute to the identification of the neuro-SNs with highest spiking rates.

From Fig. 7 we also see that TDR becomes larger as the number of scheduled nodes  $C_{\max}$  increases, demonstrating the importance of collecting information from multiple neuro-SNs. This is because by calculating e-value (18) based on the spike rate from multiple nodes, the reader can mitigate the negative impact of small e-value caused by the selection of nodes having small spike rate in anomalous state,  $q_1^k$ .

### D. Impact of System Parameters

In this subsection, we focus on the performance of track-and-stop scheduling, evaluating the impacts of different system parameters.

1) *On the FDR constraint  $\alpha$ :* Fig. 8 shows the FDR and TDR as a function of FDR constraint  $\alpha$ . The figure highlights the trade-off between TDR and FDR: as the allocated FDR constraint  $\alpha$  becomes larger, the reader can more easily detect anomalies, increasing the TDR. We can also see that TDR becomes larger as the forgetting factor  $\delta$  becomes smaller. In fact, with a smaller  $\delta$ , the FDR constraint puts higher weight on the results of the latest decisions, decreasing the importance of past false alarms.

2) *On the sensitivity of the sensors:* We now study the dependence of the system performance on the parameter defining the quality of the observations of sensors. First, we

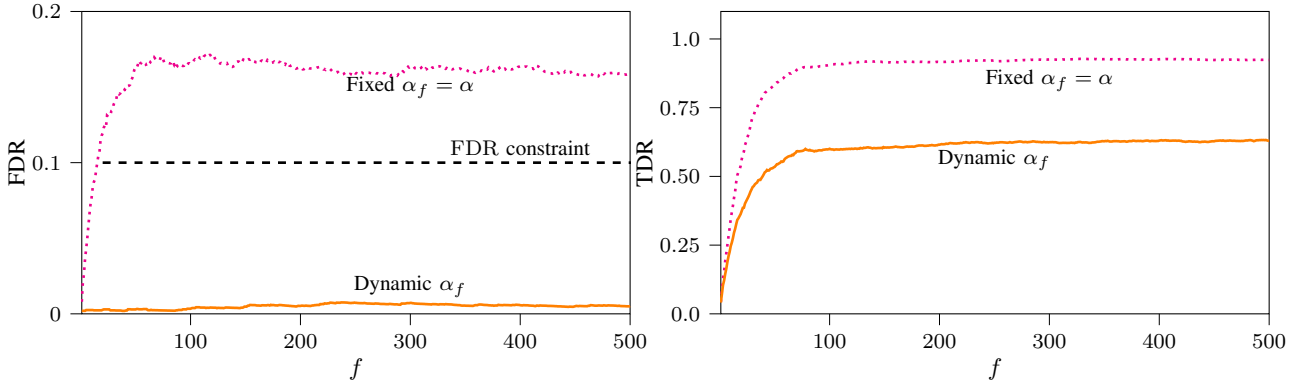


Fig. 5: FDR and TDR versus the time frame  $f$  for fixed anomaly decision threshold  $\alpha_f = \alpha$  for all  $f \in [1, F]$  and for the proposed dynamic anomaly decision threshold based on (22), where we set  $K = 1$  and  $\pi_1 = 0.05$ .

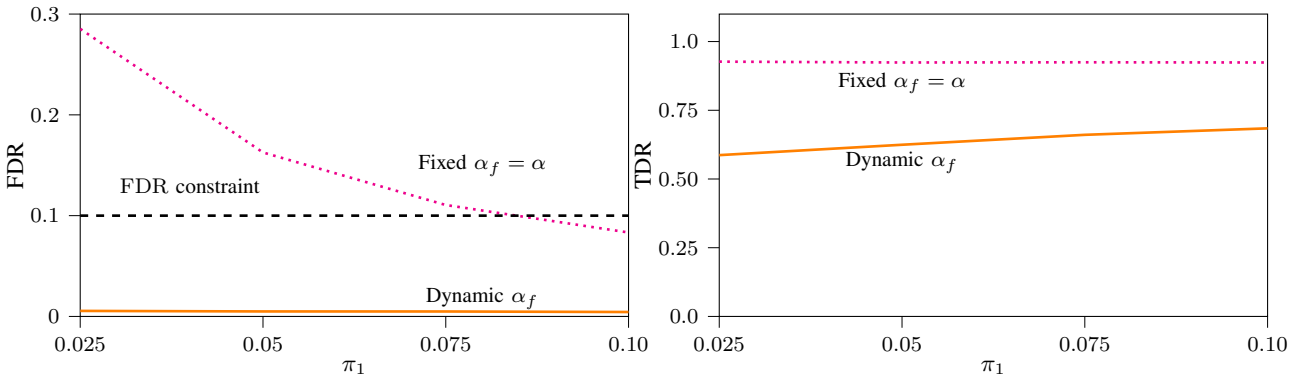


Fig. 6: FDR and TDR versus the anomaly probability  $\pi_1$  for fixed anomaly decision threshold  $\alpha_f = \alpha$  for all  $f \in [1, F]$  and for the proposed dynamic anomaly decision threshold based on (22), where we set  $K = 1$  and  $F = 1,000$ .

vary the upper bound  $\Delta_{\max}$  on the spiking rate in the presence of anomalies. From Fig. 9, we can see that TDR is improved as the upper bound  $\Delta_{\max}$  becomes larger, that is, the sensitivity improves. This is because a larger upper bound  $\Delta_{\max}$  tends to increase the difference between the spike rate of neuro-SN  $k$  in the normal state  $q_0^k$  and that in the anomalous state  $q_1^k$ , enabling the reader to detect anomalies with higher accuracy (see Fig. 3).

Fig. 10 shows the TDR as a function of the frame index  $f$  for different numbers of uplink slots  $L$ . From Fig. 10, we can see that TDR becomes larger as  $L$  increases because the reader can execute anomaly detection task based on more number of received spikes, realizing accurate decision based on the e-value in (18) and decision threshold defined in (22). For example, to achieve TDR larger than 0.9 under  $\Delta_{\max} = 0.5$ , there is a need for  $L = 100$  uplink slots.

3) *Impact of anomaly probability  $\pi_1$ :* Fig. 11 shows TDR against  $f$  for track-and-stop, where we set the anomaly probability to  $\pi_1 = \{0.05, 0.10, 0.15\}$ . As  $\pi_1$  increases, the probability that the reader obtains the higher e-value in the single frame also increases, making it more likely that the reader rejects the hypothesis at the current frame. As a result, we can see that TDR increases as  $\pi_1$  becomes larger.

4) *On the channel error rate:* To evaluate the impact of channel error in the binary asymmetric channel described in Sec. II-C, we vary the error probability  $\epsilon$ , by setting: (i)  $\epsilon_{01} = \epsilon$  and  $\epsilon_{10} = 0$ ; (ii)  $\epsilon_{10} = \epsilon$  and  $\epsilon_{01} = 0$ ; (iii)  $\epsilon_{01} = \epsilon_{10} = \epsilon$ . From Fig. 12, we see that the error probability  $\epsilon_{10}$  has the largest impact on TDR. In fact, as increase in  $\epsilon_{10}$  causes spike losses, which may be critical for anomaly detection. Conversely, as the error probability  $\epsilon_{01}$  increases, it becomes more likely that the reader mistakenly detects false spikes, causing the reader to mistakenly detect an anomaly event when the environment is in a normal state. As the reader must satisfy the FDR constraint in (9), in this case the reader must take a conservative decision when the actual anomaly event happens, reducing the TDR. When both errors have a non-zero probability, it is affected by both spike losses and falsely detected spikes, causing further decreases in the TDR.

## VI. CONCLUSION

This paper proposed a low-power online anomaly detection framework for neuromorphic wireless sensor networks. We have introduced an algorithm that can control the false discovery rate by incorporating e-values test statistics calculated based on the received spike sequences at each frame. We have also introduced a track-and-stop methods for scheduling nodes

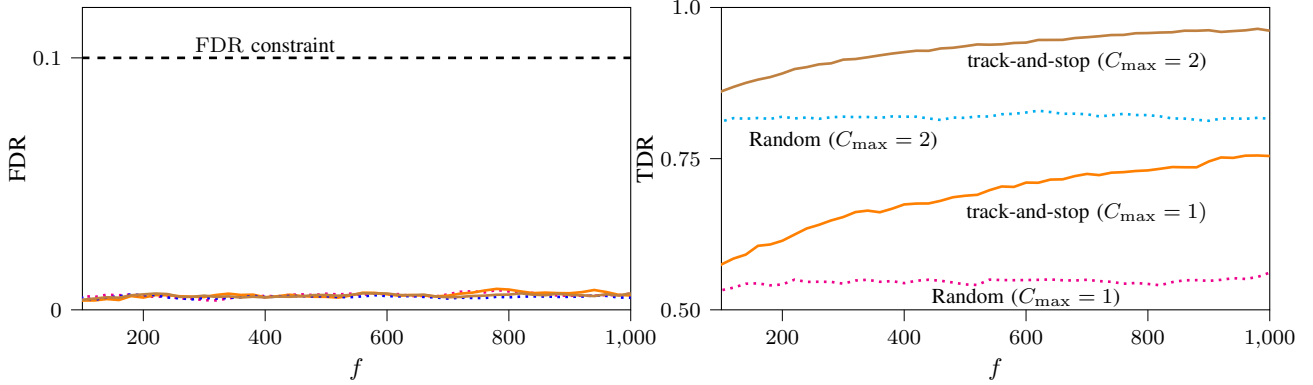


Fig. 7: FDR and TDR versus the time frame  $f$  for random sampling scheme and track-and-stop.

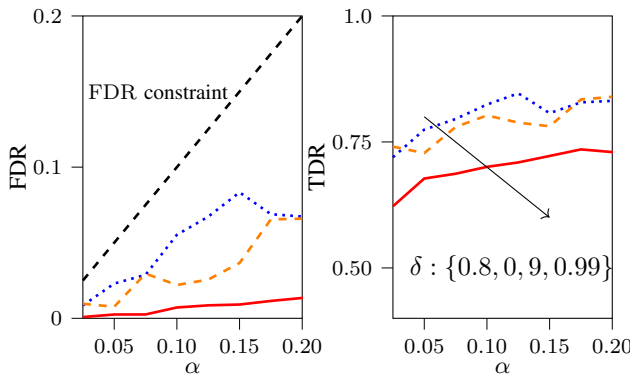


Fig. 8: FDR and TDR versus the FDR constraint  $\alpha$  for track-and-stop (the forgetting factor  $\delta = \{0.8, 0.9, 0.99\}$ ).

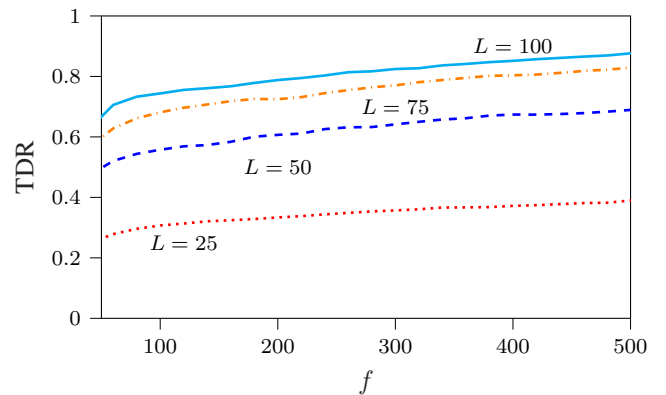


Fig. 10: TDR versus the time frame  $f$  for track-and-stop with different values of the number of uplink slots  $L$ .

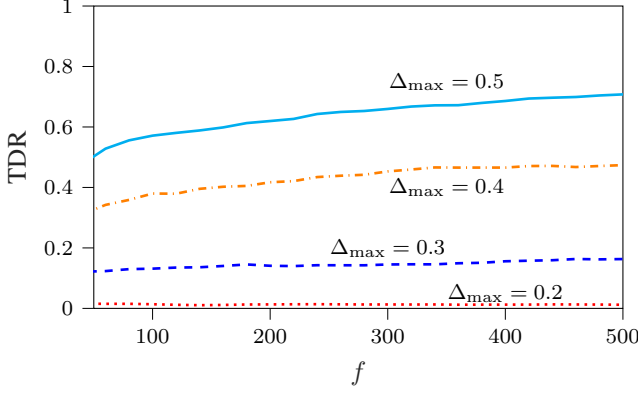


Fig. 9: TDR versus the time frame  $f$  for track-and-stop with different values of upper bound of sensor reading  $\Delta_{\max}$ .

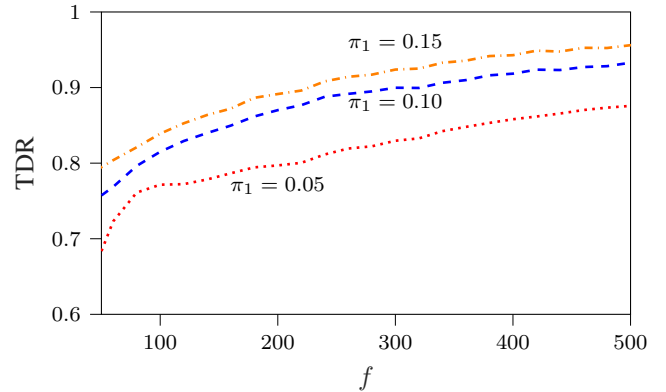


Fig. 11: TDR versus the time frame  $f$  for track-and-stop scheme with different values of anomaly portion  $\pi_1 = \{0.05, 0.10, 0.15\}$

based on the channel constraint. Our numerical results show that the proposed approach can track the nodes having the largest spike efficiently with high TDR, while maintaining the FDR below the predetermined threshold.

Future work includes designing pull-based communication protocol in neuromorphic communication while taking into account aspects such as information freshness and value of information. Designing neuromorphic communication proto-

cols for heterogeneous neuro-SNs with different capabilities in terms of sensing and communication is also an interesting research avenue.

## REFERENCES

[1] P. Lichtsteiner, C. Posch, and T. Delbrück, “A 128 x 128 120db 30mw asynchronous vision sensor that responds to relative intensity change,”

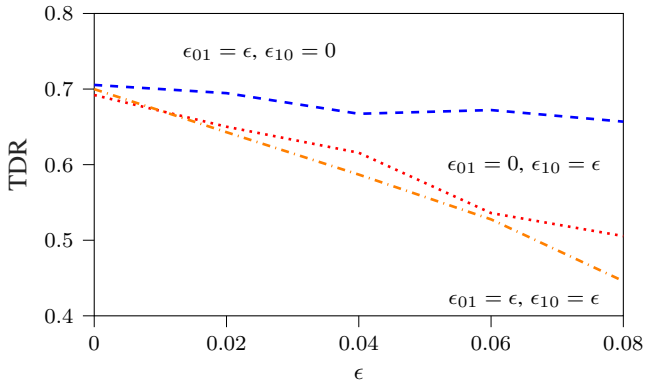


Fig. 12: TDR versus error rate  $\epsilon$  for track-and-stop.

in 2006 IEEE Int. Solid State Circuits Conf. Dig. Tech. Papers, 2006, pp. 2060–2069.

- [2] M. Martini, J. Adhuran, and N. Khan, “Lossless compression of neuromorphic vision sensor data based on point cloud representation,” *IEEE Access*, vol. 10, pp. 121 352–121 364, 2022.
- [3] M. Davies, N. Srinivasa, T.-H. Lin, G. Chinya, Y. Cao, S. H. Choday, G. Dimou, P. Joshi, N. Imam, S. Jain *et al.*, “Loihi: A neuromorphic manycore processor with on-chip learning,” *IEEE Micro*, vol. 38, no. 1, pp. 82–99, 2018.
- [4] S.-C. Liu, T. Delbruck, G. Indiveri, A. Whatley, and R. Douglas, *Event-based neuromorphic systems*. John Wiley & Sons, 2014.
- [5] J. Chen, N. Skatchkovsky, and O. Simeone, “Neuromorphic wireless cognition: event-driven semantic communications for remote inference,” *IEEE Trans. Cogn. Commun. Netw.*, vol. 9, no. 2, pp. 252–265, 2023.
- [6] N. Skatchkovsky, H. Jang, and O. Simeone, “End-to-end learning of neuromorphic wireless systems for low-power edge artificial intelligence,” in *Proc. 2020 54th Asilomar Conf. Signals Syst. Comput.*, 2020, pp. 166–173.
- [7] J. Chen, S. Park, P. Popovski, H. V. Poor, and O. Simeone, “Neuromorphic split computing with wake-up radios: Architecture and design via digital twinning,” *IEEE Trans. Signal Process.*, vol. 72, pp. 4635–4650, 2024.
- [8] J. Chen, N. Skatchkovsky, and O. Simeone, “Neuromorphic integrated sensing and communications,” *IEEE Wireless Commun. Lett.*, vol. 12, no. 3, pp. 476–480, 2022.
- [9] D. Wu, J. Chen, B. Rajendran, H. Vincent Poor, and O. Simeone, “Neuromorphic wireless split computing with multi-level spikes,” *IEEE Trans. Mach. Learn. Commun. Netw.*, vol. 3, pp. 502–516, 2025.
- [10] J. Lee, A.-H. Lee, V. Leung, F. Laiwalla, M. A. Lopez-Gordo, L. Larson, and A. Nurmikko, “An asynchronous wireless network for capturing event-driven data from large populations of autonomous sensors,” *Nature Electron.*, vol. 7, no. 4, pp. 313–324, 2024.
- [11] S. Schaefer, D. Gehrig, and D. Scaramuzza, “AEGNN: Asynchronous event-based graph neural networks,” in *Proc. IEEE/CVF Conf. Comput. Vision Pattern Recognit.*, 2022, pp. 12 371–12 381.
- [12] G. Rak, “Salt-size sensors mimic the brain: An array of tiny wireless nodes could someday find their way into brain-machine interfaces,” [Online], <https://spectrum.ieee.org/brain-machine-interface-2667619198>.
- [13] A. A. Alkhatib, “A review on forest fire detection techniques,” *Int. J. Distrib. Sensor Netw.*, vol. 10, no. 3, p. 597368, 2014.
- [14] Q. Rebjock, B. Kurt, T. Januschowski, and L. Callot, “Online false discovery rate control for anomaly detection in time series,” *Adv. Neural Inf. Process. Syst.*, vol. 34, pp. 26 487–26 498, 2021.
- [15] S. Ahmad, A. Lavin, S. Purdy, and Z. Agha, “Unsupervised real-time anomaly detection for streaming data,” *Neurocomputing*, vol. 262, pp. 134–147, 2017.
- [16] A. Lavin and S. Ahmad, “Evaluating real-time anomaly detection algorithms—the numenata anomaly benchmark,” in *2015 IEEE 14th Int. Conf. Mach. Learn. Appl. (ICMLA)*. IEEE, 2015, pp. 38–44.
- [17] A. Javanmard and A. Montanari, “Online rules for control of false discovery rate and false discovery exceedance,” *Ann. Statist.*, vol. 46, no. 2, pp. 526–554, 2018.
- [18] A. Garivier and E. Kaufmann, “Optimal best arm identification with fixed confidence,” in *Conf. Learn. Theory*. PMLR, 2016, pp. 998–1027.
- [19] Prophesee, “Event-based vision applications,” [Online], <https://www.prophesee.ai/>.
- [20] IniVation, “Extreme machine vision,” [Online], <https://inivation.com/>.
- [21] SynSens, “Speck,” [Online], <https://www.synsense.ai/products/speck-2/>.
- [22] Y. Ke, Z. Utkovski, M. Heshmati, O. Simeone, J. Dommel, and S. Stanczak, “Neuromorphic wireless device-edge co-inference via the directed information bottleneck,” in *2024 Int. Conf. Neuromorphic Syst. (ICONS)*. IEEE, 2024, pp. 16–23.
- [23] E. Kaufmann, O. Cappé, and A. Garivier, “On the complexity of best-arm identification in multi-armed bandit models,” *J. Mach. Learn. Res.*, vol. 17, no. 1, pp. 1–42, 2016.
- [24] Y. Zhang, O. Simeone, S. T. Jose, L. Maggi, and A. Valcarce, “Bayesian and multi-armed contextual meta-optimization for efficient wireless radio resource management,” *IEEE Trans. Cogn. Commun. Netw.*, vol. 9, no. 5, pp. 1282–1295, 2023.
- [25] A. Ramdas and R. Wang, “Hypothesis testing with e-values,” *arXiv preprint arXiv:2410.23614*, 2024.
- [26] J. Shiraishi, S. Cavallero, S. R. Pandey, F. Saggese, and P. Popovski, “Coexistence of push wireless access with pull communication for content-based wake-up radios,” in *GLOBECOM 2024 - 2024 IEEE Global Commun. Conf.*, 2024, pp. 4836–4841.